PNAS
www.pnas.org

Supplementary Information for

GEF mechanism revealed by the structure of SmgGDS-558 and farnesylated RhoA complex and its implication for chaperone mechanism

Hikaru Shimizu[1], Sachiko Toma-Fukai[1], Kenji Kontani[2], Toshiaki Katada[3] and Toshiyuki Shimizu[1*]

[1] Graduate School of Pharmaceutical Sciences, The University of Tokyo, 7-3-1 Hongo, Bunkyo-ku, Tokyo 113-0033, Japan.
[2] Department of Biochemistry, Meiji Pharmaceutical University, 2-522-1 Noshio, Kiyose-shi, Tokyo 204-8588, JAPAN
[3] Faculty of Pharmacy, Musashino University, 1-1-20 Shin-machi, Nishitokyo-shi, Tokyo 202-0023, JAPAN

Correspondence to: Toshiyuki Shimizu
E-mail: shimizu@mol.f.u-tokyo.ac.jp
Tel: (+81) 03-5841-4840; Fax: (+81) 03-5841-4891

This PDF file includes:

www.pnas.org/cgi/doi/10.1073/pnas.1804740115

Extended acknowledgments

We thank all beamline staffs at BL41XU and BL44XU of SPring-8, BL1A of Photon Factory for helping and kindly suggestion about experiment. Especially, we thank Keitaro Yamashita and Kazuya Hasegawa for instruction about KAMO analysis. A part of this work was performed using synchrotron beamline BL44XU at SPring-8 under the Cooperative Research Program of the Institute for Protein Research, Osaka University (2016B6626, 2017A6730 and 2017B6730). This research is partially supported by Platform Project for Supporting Drug Discovery and Life Science Research (Basis for Supporting Innovative Drug Discovery and Life Science Research (BINDS)) from Japan Agency for Medical Research and Development (AMED) under Grant Number JP18am0101070.

Material and Method

Preparation of recombinant SmgGDS, non-prenylated RhoA in *E*.coli

Both isoforms of human SmgGDS (wild type and mutants) and non-prenylated human RhoA (wild type and mutants) were produced in *E.coli* as previously described (1).

Preparation of recombinant post-translationally modified RhoA *in vitro*

Non-prenylated $RhoA^{L193A}$ was farnesylated *in vitro* as previously described (2).

Crystallization of SmgGDS-558/ farnesylated RhoA complex

Crystallization was performed with sitting drop vapor-diffusion method. Separately purified SmgGDS-558 and farnesylated RhoA were mixed with 1:1 molar ratio and diluted to 5 mg/mL with buffer D (150 mM NaCl, 20 mM Tris-HCl pH 7.5, 1 mM DTT, 5 mM EDTA). The same volume of protein solution and reservoir solution (0.2 M sodium malonate pH 6.0 and 20% (w/v) PEG3350) were mixed at 10˚C. Rhombic crystals were found in a week and they were grown for several months.

Data collection and structure determination of SmgGDS-558/ farnesylated RhoA complex

X-ray diffraction data set of SmgGDS-558/farnesylated RhoA crystal was collected on beamline BL44XU at SPring-8 (Hyogo, Japan) 30% (w/v) glycerol-containing reservoir solution was used as cryoprotectant. Because the electron density map (occupancy) of prenyl group was varied by crystal, we collected a large number of diffraction image data and selected a merged data with a high occupancy of prenyl group. All diffraction datasets were automatically processed using the program KAMO (3). The 246 files including diffraction scan data were given to KAMO, and of these 126 were indexed and integrated with the equivalent unit cell parameters by the program XDS (4). These integrated results were subjected to hierarchical clustering based on the correlation coefficients, and in each cluster the datasets were scaled and merged by the program XSCALE with outlier rejections implemented in KAMO. The mF_o-DF_c prenyl-group omit maps of all clusters were calculated and evaluated. We selected the best cluster which is derived from 2 crystals and give clear electron density of all prenyl groups in an asymmetric unit. Molecular replacement was performed with the program Molrep (5). Manual model building was performed with the program coot (6). The model structure

was refined with the program Refmac5 (7) and Phenix (8). Geometry of the final structure was checked with the program PROCHECK (9). Measurement summary and statistics of crystallographic data are summarized in Table S1. Coordinates and the structure factor of SmgGDS-558/farnesylated hRhoA were deposited in the Protein Data Bank (PDB ID: 5ZHX). All diffraction images were deposited in the Zenodo data repository (https://doi.org/10.5281/zenodo.1134209). CueMol2 was used for structural drawing in this paper (http://www.cuemol.org/en/). The amino acid residues interacting farnesylated C190 was selected with program LIGPLOT(+) (10).

Pulldown assay

GST-SmgGDS and His_6 -RhoA were used for pulldown assay. This assay was performed in a Mg^{2+} ion free condition with buffer D. 3 nmol of each protein and 100 uL of resin (cOmplete His-Tag Purification Resin) were mixed and incubated at 4 ˚C for 1 hour. After washing, proteins were eluted with elution buffer (300 mM imidazole containing buffer D). Eluted samples were analyzed by sodium dodecyl sulfate polyacrylamide gel electrophoresis (SDS–PAGE). Each gel was stained with Coomassie Brilliant Blue.

Guanine-nucleotide dissociation assay

The guanine-nucleotide dissociation rate was measured by FLUOstar OPTIMA (BMG LABTECH). 200 µL of BODYPY-loaded RhoA (0.2 µM final conc.) was mixed with 20 µL of reaction reagent containing 5 mM GMPPNP and 0.4 µM of each type of SmgGDS. The dissociation assays were performed at 37˚C with λex = 485 nm and λem = 520 nm. Each assay was measured three times and analyzed with GraFit ver7. For non-farnesylated RhoA analysis, all measured values were used for calculating GDP dissociation rate. For farnesylated RhoA, first 10 measured values were used. The dissociation rate of farnesylated or non-farnesylated RhoA without SmgGDS was used as control.

Docking simulation by AUTODOCK4

Docking simulation of S-geranylgeranylated cysteine was performed by program AUTODOCK4 (11, 12). SmgGDS-558 in complex II was used as rigid protein model for this simulation. The simulation performed 1000 runs and model which has the lowest binding energy was selected as result.

Homology modeling by MODELLER

Homology model of SmgGDS-607 was calculated by MODELLER 9.18 program (13-16). To build homology model, the sequence alignment and crystal structures of SmgGDS-558 (PDB ID: 5XGC) and beta-catenin (PDB ID: 1TH1) were used as input data. SmgGDS-607 (aa 77-607) was aligned to SmgGDS-558 (aa 122-558) and beta-catenin (aa 145-664) with program BLAST (17).

Modeling of protein-peptide interaction by CABS-dock web server

The binding interface between SmgGDS-607 (Homology model) and RhoA PBR was determined by the CABS-dock server (http://biocomp.chem.uw.edu.pl/CABSdock) (18, 19).

Isothermal Titration Calorimetry

ITC experiments were carried out at 25˚C in the buffer condition of 20 mM Hepes pH 7.5 and 150 mM NaCl by using MicroCal iTC200 (GE Healthcare). 50 μM of SmgGDS-607 (wild type or each mutant) was titrated by 500, 1000 or 2000 μM of RhoA PBR-CaaX peptide (ARRGKKSGCLVL). The titration sequence included a single 0.4 μL injection followed by 18 injections, 2 μL each.

Supplymentary Figures

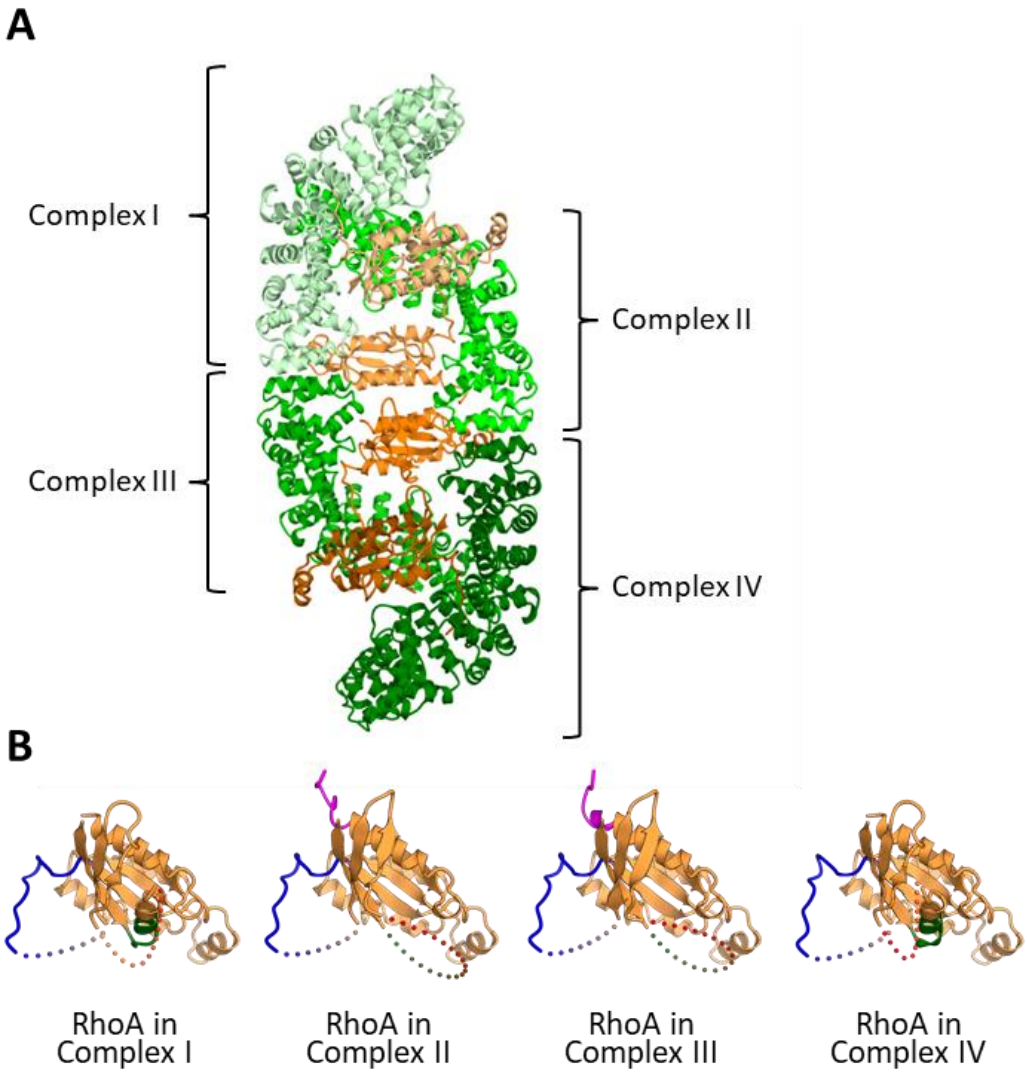

Fig. S1 Complex structure in an asymmetric unit
A, Whole complex structures in an asymmetric unit. SmgGDS-558 and RhoA are shown in green and orange, respectively.
B, Comparison of RhoA structure with each complex (complex I-IV). Disordered region is shown as dotted lines.

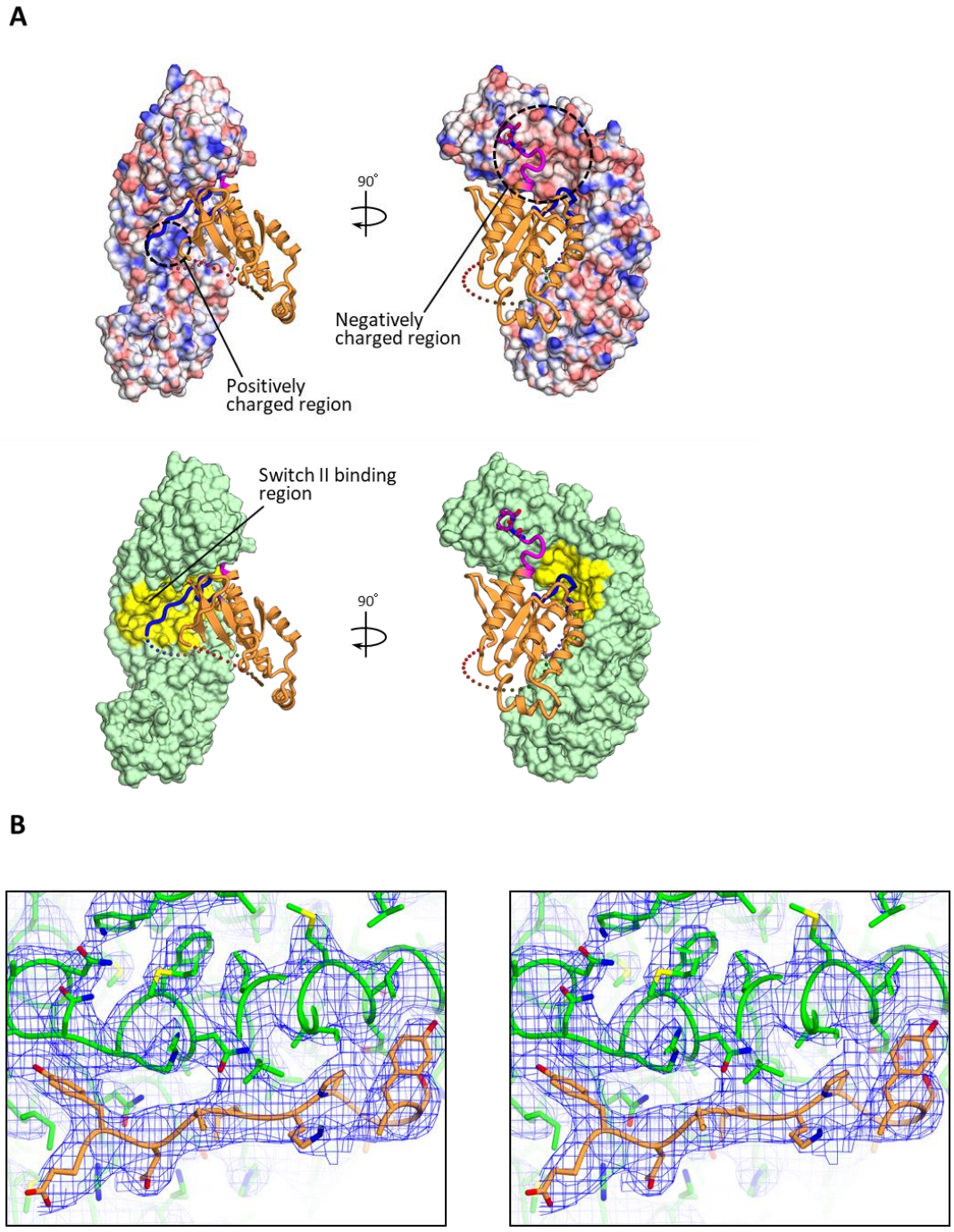

Fig. S2 Surface model of SmgGDS-558 in complex structure and electron density map around the switch II binding region

A, Electrostatic surface potential map and surface model of SmgGDS-558. RhoA is shown as ribbon model. (Upper) The positively charged region and the negatively charged region are enclosed by dotted circle. (Lower) The switch II binding region is mapped in yellow on the surface model.

B, Stereo view of experimental electron density map around the switch II binding region. The 2mFo-DFc electron density map (contoured at 1.0 σ) is shown. The side chain residues of SmgGDS-558 and RhoA are shown in stick model, and colored in green and orange, respectively.

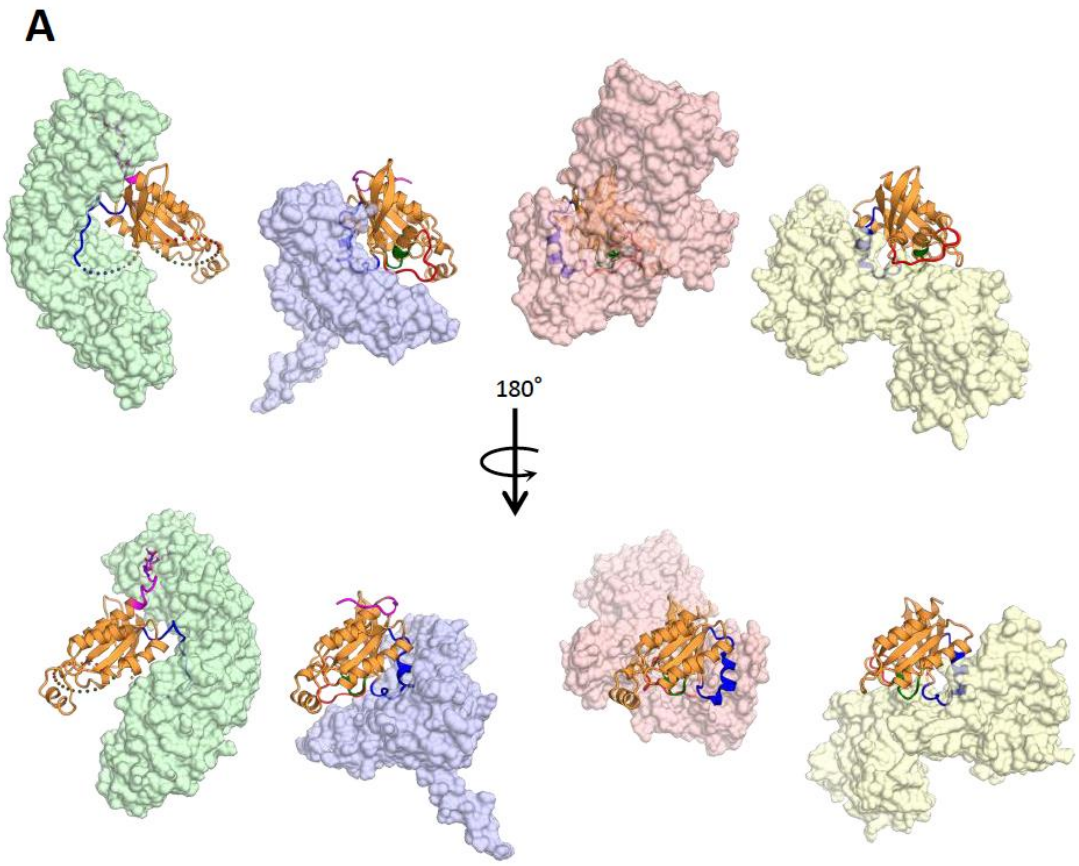
A
180°
hSmgGDS/hRhoA
Complex
PDBID: 5ZHX
1816.8 Å²
mDbs/hCdc42
Complex
PDBID: 1KZ7
1684.9 Å²
hDock9/hCdc42
Complex
PDBID: 2WM9
2307.7 Å²
hSos1/hH-Ras
Complex
PDBID: 1BKD
1643.4 Å²

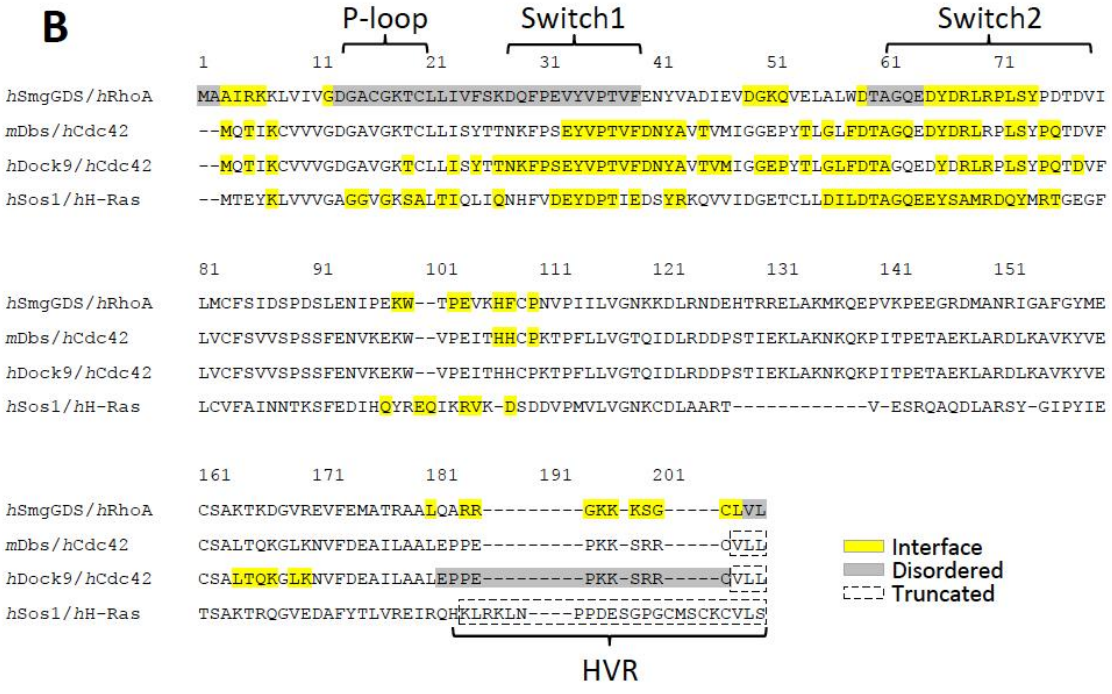
B
P-loop
Switch1
Switch2
hSmgGDS/hRhoA MAAIRKKLVIVGDGACGKTCLLIVFSKDQFPEVYVPTVFENYVADIEVDGKQVELALWDTAGQEDYDRLRPLSYPDTDVI
mDbs/hCdc42 --MQTIKCVVVGDGAVGKTCLLISYTTNKFPSEYVPTVFDNYAVTVMIGGEPYTLGLFDTAGQEDYDRLRPLSYPQTDVF
hDock9/hCdc42 --MQTIKCVVVGDGAVGKTCLLISYTTNKFPSEYVPTVFDNYAVTVMIGGEPYTLGLFDTAGQEDYDRLRPLSYPQTDVF
hSos1/hH-Ras --MTEYKLVVVGAGGVGKSALTIQLIQNHFVDEYDPTIEDSYRKQVVIDGETCLLDILDTAGQEEYSAMRDQYMRTGEGF
hSmgGDS/hRhoA LMCFSIDSPDSLENIPEKW--TPEVKHFCPNVPIILVGNKKDLRNDEHTRRELAKMKQEPVKPEEGRDMANRIGAFGYME
mDbs/hCdc42 LVCFSVVSPSSFENVKEKW--VPEITHHCPKTPFLLVGTQIDLRDDPSTIEKLAKNKQKPITPETAEKLARDLKAVKYVE
hDock9/hCdc42 LVCFSVVSPSSFENVKEKW--VPEITHHCPKTPFLLVGTQIDLRDDPSTIEKLAKNKQKPITPETAEKLARDLKAVKYVE
hSos1/hH-Ras LCVFAINNTKSFEDIHQYREQIKRVK-DSDDVPMVLVGNKCDLAART----------V-ESRQAQDLARSY-GIPYIE
hSmgGDS/hRhoA CSAKTKDGVREVFEMATRAALQARR---------GKK-KSG-----CLVL
mDbs/hCdc42 CSALTQKGLKNVFDEAILAALEPPE---------PKK-SRR-----QVLL
hDock9/hCdc42 CSALTQKGLKNVFDEAILAALEPPE---------PKK-SRR-----QVLL
hSos1/hH-Ras TSAKTRQGVEDAFYTLVREIRQHKLRKLN----PPDESGPGCMSCKCVLS
Interface
Disordered
Truncated
HVR

Fig. S3 Comparison of GEF/small GTPase complex structure
A, Crystal structures of four GEF/small GTPase complexes (PDBID: 5ZHX, 1KZ7, 2WM9, 1BKD). Small GTPases are shown as ribbon model and GEFs are shown as surface model. All small GTPases are displayed in the same orientation. Each buried surface area is listed.
B, Sequence alignment of small GTPases in GEF complex. The amino acid residues forming interface are highlighted in yellow. Disordered residues are highlighted in grey and residues truncated for crystallization are enclosed by dotted line. The interface analysis was performed using PISA.

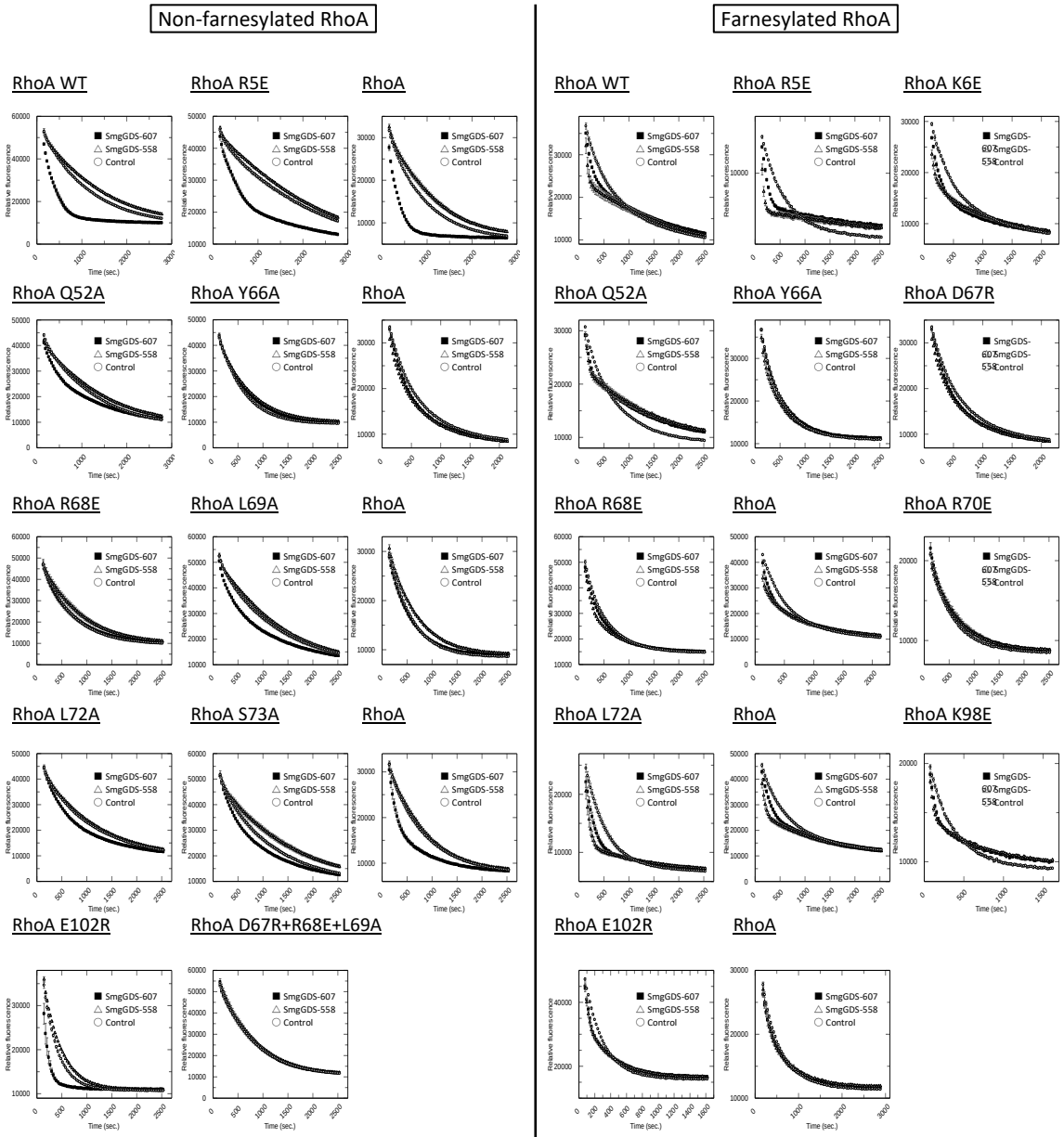

Fig. S4 GEF assay of SmgGDS for RhoA and its mutants

GEF assay, related to Fig. 3B. Guanine nucleotide dissociation was measured by monitoring fluorescence from BODYPY-GDP bound non-farnesylated/farnesylated RhoA. The same assay was performed three times and each plot represented the average value of fluorescence. The fluorescence decay curves of SmgGDS-558, SmgGDS-607 and control are shown as white circle, black square and white triangle, respectively. Standard error is shown as error bar.

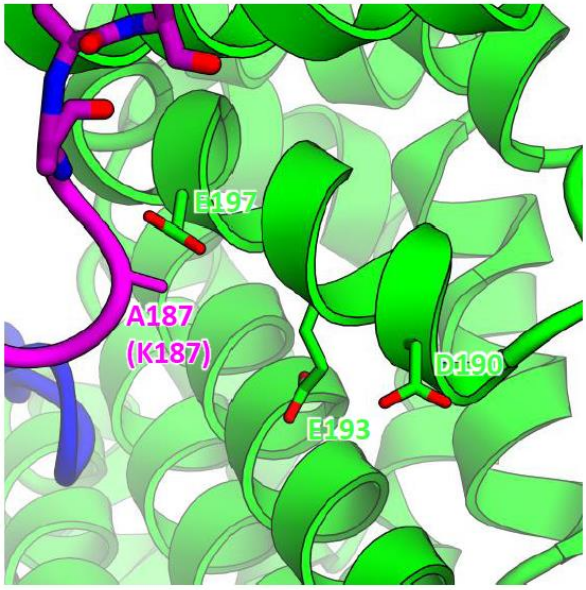

Fig. S5 Enlarged view of the crystal structure around K187 of RhoA
The structure around K187 of RhoA is shown. K187 is modeled as Ala due to the poor electron density. D190, E193 and E197 in SmgGDS-558, which corresponded to D239, E242 and E246 in SmgGDS-607, are shown as stick model.

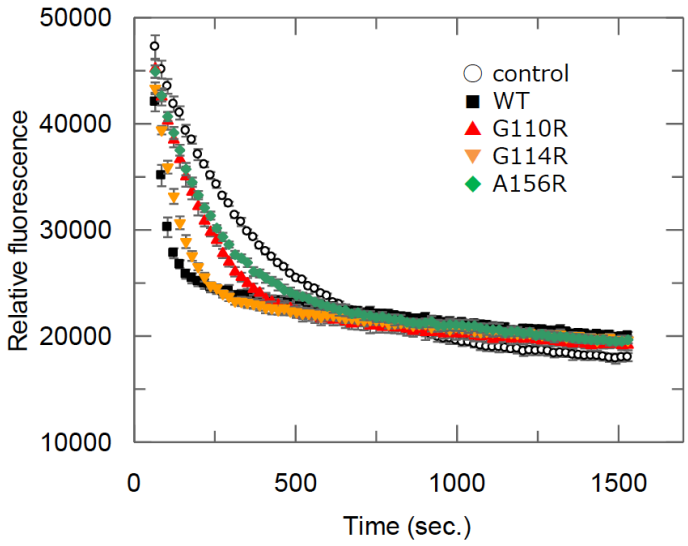

Fig. S6 GEF assay of SmgGDS-558 and its mutant for farnesylated RhoA
GEF assay, related to Fig. 4D. Guanine nucleotide dissociation was measured by monitoring fluorescence from BODYPY-GDP bound farnesylated RhoA. The same assay was performed three times and each plot represented the average value of fluorescence. The fluorescence decay curves of series of SmgGDS-558 and control are shown. Standard error is shown as error bar.

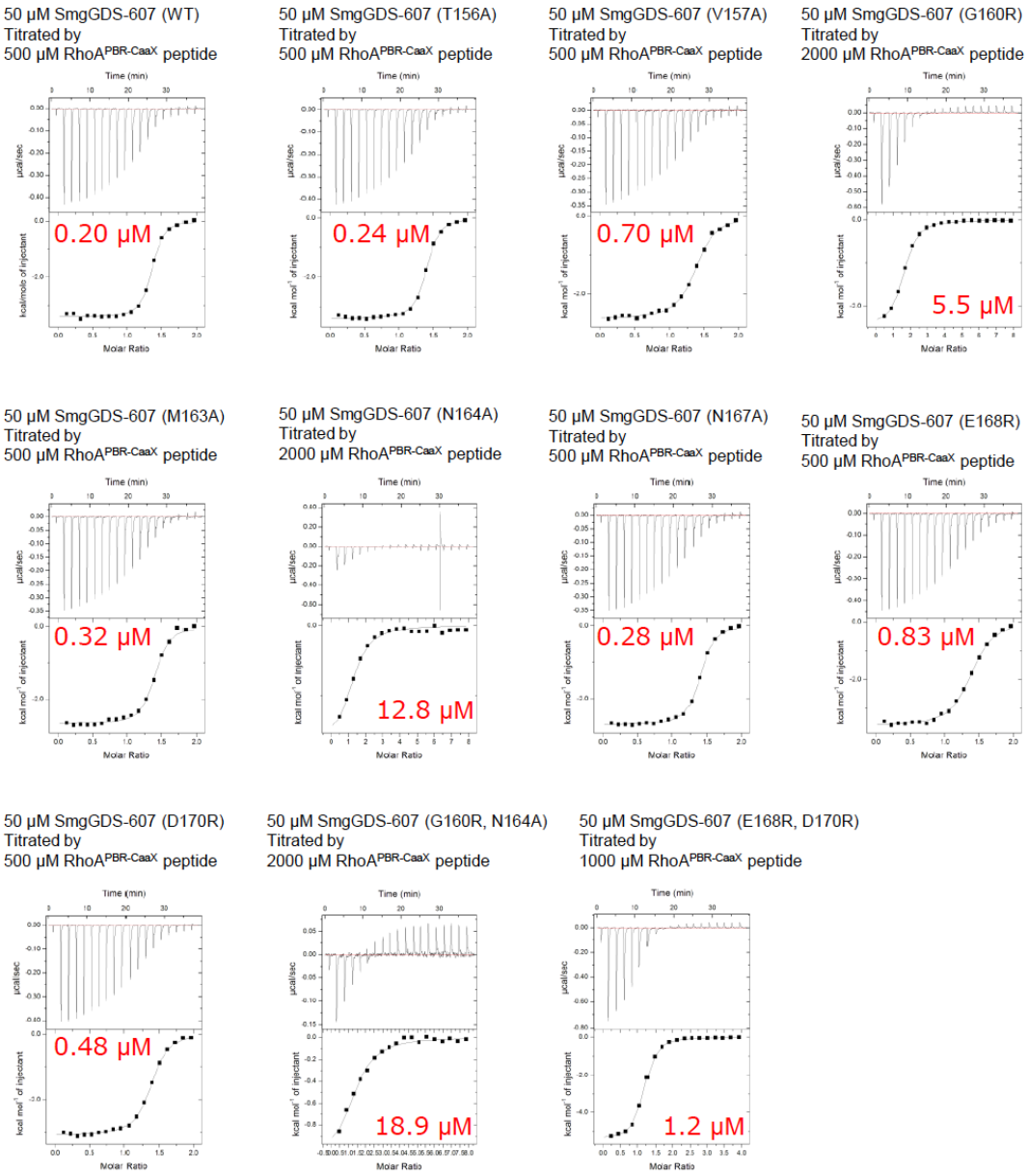

Fig. S7 ITC thermograms
ITC thermograms, related to Table S2. Each K_d value is shown in the panel.

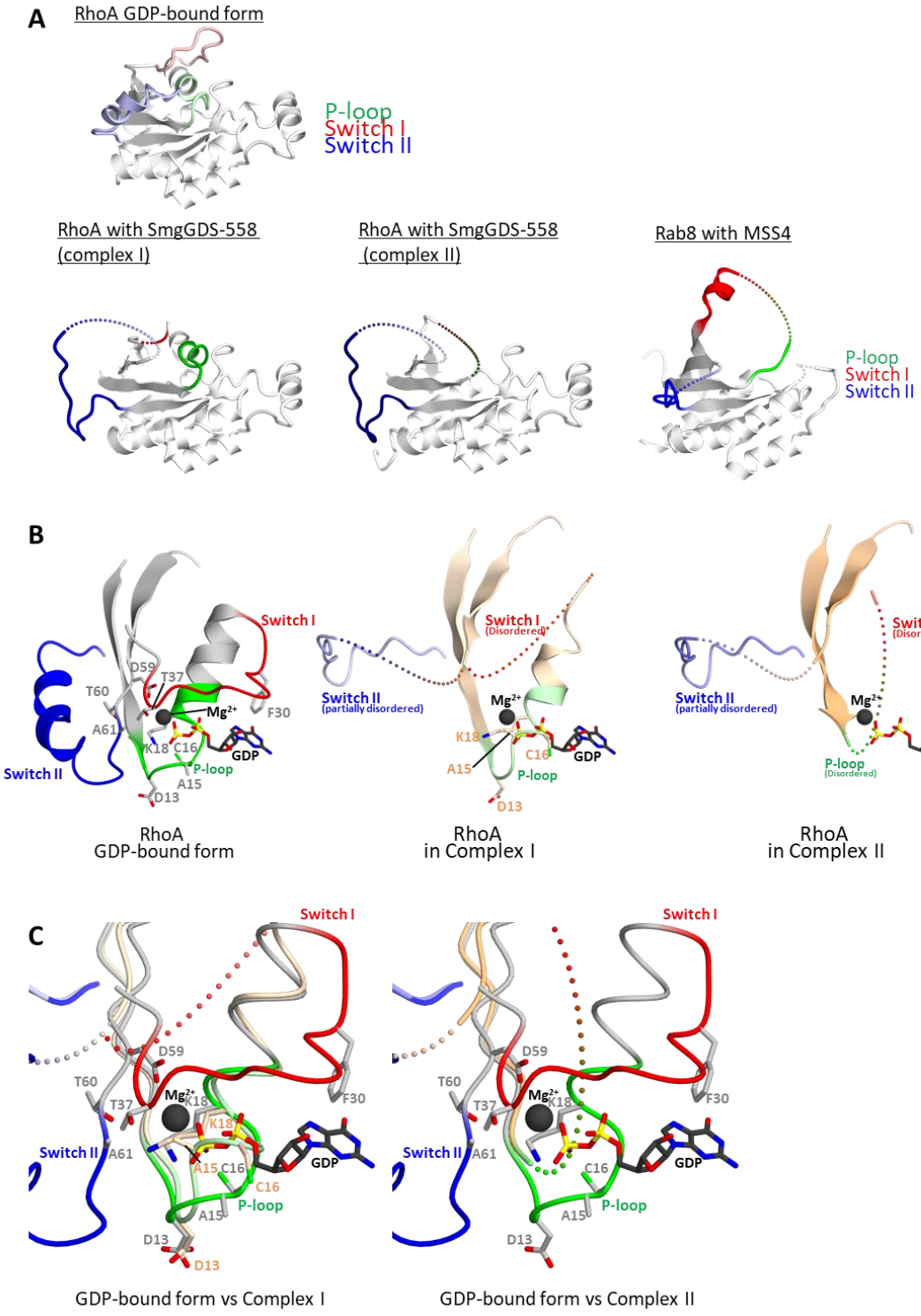
A
RhoA GDP-bound form
P-loop
Switch I
Switch II
RhoA with SmgGDS-558 (complex I)
RhoA with SmgGDS-558 (complex II)
Rab8 with MSS4
P-loop
Switch I
Switch II
B
Switch I
Switch II
D59
T37
T60
Mg2+
F30
A61
K18
C16
GDP
P-loop
A15
D13
Switch I (Disordered)
Switch II (partially disordered)
RhoA GDP-bound form
RhoA in Complex I
RhoA in Complex II
C
GDP-bound form vs Complex I
GDP-bound form vs Complex II

Fig. S8 Structural details of RhoA in complex structure
A, Structural comparison between RhoA and Rab8 in the complex structure. The crystal structure of RhoA GDP-bound form (PDB ID: 1FTN) is shown (upper) and RhoA in complex with SmgGDS-558 (complex I and II) and Rab8 in complex with MSS4 (PDB ID: 2FU5) are shown (lower). P-loop switch I, and switch II are colored in green, red and blue, respectively.
B, Structural comparison of Mg ion and GDP-bound RhoA (PDB ID: 1FTN, right) with Mg ion and GDP-free RhoA in complex I (middle) and complex II (right). Structure around G1, G2 and G3 is shown as ribbon model. Mg ion and GDP of 1FTN are overlaid on RhoA structure in complex I and II. Side chains of G1, G2 and part of switch II (F30 and T37) are shown as stick model. RhoA of complex I and II are colored in orange. RhoA of 1FTN are colored in gray. P-loop, switch I and switch II in all RhoAs are colored in green, red and blue, respectively.
C, Superposition of GDP binding site of RhoA of 1FTN and complex I (left) and II (right). Side chains of G1, G2 and part of switch II (F30 and T37) of RhoA are shown as stick model.

Table S1. Crystallographic statistics.

	SmgGDS-558/farnesylated RhoA
Space group	$P2_12_12_1$
Wavelength (Å)	0.90000
No. of crystals	2
Unit cell (*a*, *b*, *c*)	93.3, 181.8, 205.3
X-ray source	SPring-8 BL44XU
Resolution (Å) (outer shell)	136.1-3.5 (3.71-3.50)[a]
No. of obs. ref.	1967740
No. of unique. ref.	44892
Completeness (%)	99.9 (100.0)
R_{meas}[b]	0.565 (4.100)
$I/\sigma(I)$	10.4 (1.2)
CC1/2	0.997 (0.623)
< Refinement >	
Resolution (Å)	136.1-3.5
R_{work} (%)[c]	25.0
R_{free} (%)[d]	30.6
RMSD	
Bond length (Å)	0.009
Bond angles (˚)	1.420
Number of atoms per asymmetric unit	
Protein	18728
Ligand	0
Ramachandran plots	
Favored	2322 (94%)
Allowed	149 (6%)
Outlier	5 (0%)

[a] The numbers in parentheses represent statistics in the highest resolution shell.

[b] $R_{meas}=\Sigma(n/n-1)^{1/2}\Sigma_j|<I(h)> - I(h)_j|/\Sigma\Sigma_{j|}<I(h)>$, where <I(h)> is the mean intensity of symmetry-equuivalent reflections.

[c] $R_{work}=\Sigma||F_o|-|F_c||/\Sigma|F_o|$, where F_o and F_c are the observed and calculated structure factors for data used for refinement, respectively.

[d] $R_{free}=\Sigma||F_o|-|F_c||/\Sigma|F_o|$ for 5% of the data not used at any stage of structural refinement.

Table S2. Isothermal Titration Calorimetry Data

Cell (SmgGDS-607)		Titrant (RhoA$^{PBR\text{-}CaaX}$ peptide)				
Type	Conc. (μM)	Conc. (μM)	K_d (μM)	ΔH (kcal/M)	ΔS (cal/mol/deg)	N
WT	50	500	0.20	-3.4	19.2	1.31
T156A	50	500	0.24	-3.4	18.9	1.36
V157A	50	500	0.70	-2.6	19.3	1.42
G160R	50	2000	5.5	-2.5	15.8	1.52
M163A	50	500	0.32	-2.6	20.7	1.36
N164A	50	2000	12.8	-1.7	16.5	1.19
N167A	50	500	0.28	-2.7	20.9	1.36
E168R	50	500	0.83	-3.6	15.7	1.35
D170R	50	500	0.48	-3.1	18.6	1.34
G160R, N164A	50	2000	18.9	-1.1	17.7	1.33
E168R, D170R	50	1000	1.2	-5.4	8.9	1.11

References

1. Shimizu H, *et al.* (2017) Structure-based analysis of the guanine nucleotide exchange factor SmgGDS reveals armadillo-repeat motifs and key regions for activity and GTPase binding. *The Journal of biological chemistry* 292(32):13441-13448.
2. Kuhlmann N, *et al.* (2016) Structural and Mechanistic Insights into the Regulation of the Fundamental Rho Regulator RhoGDIalpha by Lysine Acetylation. *The Journal of biological chemistry* 291(11):5484-5499.
3. Yamashita K, Hirata K, & Yamamoto M (2018) KAMO: towards automated data processing for microcrystals. *Acta Crystallogr D* 74:441-449.
4. Kabsch W (2010) Xds. *Acta Crystallographica Section D: Biological Crystallography* 66(2):125-132.
5. Vagin A & Teplyakov A (1997) MOLREP: an automated program for molecular replacement. *Journal of applied crystallography* 30(6):1022-1025.
6. Emsley P & Cowtan K (2004) Coot: model-building tools for molecular graphics. *Acta Crystallographica Section D: Biological Crystallography* 60(12):2126-2132.
7. Murshudov GN, Vagin AA, & Dodson EJ (1997) Refinement of macromolecular structures by the maximum-likelihood method. *Acta Crystallographica Section D: Biological Crystallography* 53(3):240-255.
8. Adams PD, *et al.* (2010) PHENIX: a comprehensive Python-based system for macromolecular structure solution. *Acta Crystallogr D* 66:213-221.
9. Laskowski RA, MacArthur MW, Moss DS, & Thornton JM (1993) PROCHECK: a program to check the stereochemical quality of protein structures. *Journal of applied crystallography* 26(2):283-291.
10. Laskowski RA & Swindells MB (2011) LigPlot+: Multiple Ligand-Protein Interaction Diagrams for Drug Discovery. *J Chem Inf Model* 51(10):2778-2786.
11. Morris GM, *et al.* (1998) Automated docking using a Lamarckian genetic algorithm and an empirical binding free energy function. *Journal of computational chemistry* 19(14):1639-1662.
12. Morris GM, *et al.* (2009) AutoDock4 and AutoDockTools4: Automated docking with selective receptor flexibility. *Journal of computational chemistry* 30(16):2785-2791.
13. Fiser A, Do RKG, & Sali A (2000) Modeling of loops in protein structures. *Protein Sci* 9(9):1753-1773.
14. Marti-Renom MA, *et al.* (2000) Comparative protein structure modeling of genes and genomes. *Annual review of biophysics and biomolecular structure* 29:291-325.
15. Sali A & Blundell TL (1993) Comparative Protein Modeling by Satisfaction of Spatial Restraints. *Journal of Molecular Biology* 234(3):779-815.
16. Webb B & Sali A (2014) Protein Structure Modeling with MODELLER. *Methods Mol Biol* 1137:1-15.
17. Altschul SF, Gish W, Miller W, Myers EW, & Lipman DJ (1990) Basic local alignment search tool. *J Mol Biol* 215(3):403-410.
18. Blaszczyk M, *et al.* (2016) Modeling of protein-peptide interactions using the CABS-dock web server for binding site search and flexible docking. *Methods* 93:72-83.

19. Kurcinski M, Jamroz M, Blaszczyk M, Kolinski A, & Kmiecik S (2015) CABS-dock web server for the flexible docking of peptides to proteins without prior knowledge of the binding site. *Nucleic acids research* 43(W1):W419-424.